Supplementary Information

Increased Importance of Aerosol-Cloud Interaction for Surface $PM_{2.5}$ Pollution Relative to Aerosol-Radiation Interaction in China with the Anthropogenic Emission Reduction

Da Gao[1, 2], Bin Zhao[1, 2, *], Shuxiao Wang[1, 2], Yuan Wang[3], Brian Gaudet[4], Yun Zhu[5], Xiaochun Wang[1, 2], Jiewen Shen[1, 2], Shengyue Li[1, 2], Yicong He[1, 2], Dejia Yin[1, 2], Zhaoxin Dong[1, 2]

[1]State Key Joint Laboratory of Environment Simulation and Pollution Control, School of Environment, Tsinghua University, 100084 Beijing, China

[2]State Environmental Protection Key Laboratory of Sources and Control of Air Pollution Complex, Beijing, 100084, China

[3]Department of Earth, Atmospheric, and Planetary Sciences, Purdue University, West Lafayette, IN, USA,

[4]Pacific Northwest National Laboratory, Richland, Washington, USA

[5]Guangdong Provincial Key Laboratory of Atmospheric Environment and Pollution Control, College of Environment and Energy, South China University of Technology, Guangzhou Higher Education Mega Center,

Guangzhou, 510006, China

*Correspondence to: Bin Zhao (bzhao@mail.tsinghua.edu.cn)

Section 1. The improvement for nitrate simulation

Before starting this work. We noted the poor ability of nitrate simulation in the WRF-Chem model. Previous studies reported that the nitrate underestimation might be attributed to the HONO underestimation (Wang et al., 2015; Xue et al., 2020). The source of HONO is originally from some gas-phase chemical reactions in the WRF-Chem, but other HONO sources are lacking, such as hydrolysis of NO_2 on humid aerosol surfaces and heterogeneous conversion of NO_2 on ground surfaces. It also has been confirmed that these reactions could occur in the atmosphere (Li et al., 2018, Liu et al., 2019). We added these four heterogeneous HONO reactions to the WRF-Chem model (Table S1). The addition of these four reactions enhances atmospheric oxidant and promotes OH radical formation, thereby promoting the formation of gaseous nitric acid through strong OH radicals reacting with NO_2. In addition, the reactions of hydrolysis of NO_2 on humid aerosol surfaces contributed extra nitric acid. More nitric acid is beneficial for nitrate formation through condensation and heterogeneous reactions. Other specific information can be found in Zhang et al. (2021).

Table S1. Heterogeneous HONO reactions added in WRF-Chem (from

Zhang et al., 2021).

number	Reaction	Reference
(1)	NO_2 + aerosol = 0.5 × HONO + 0.5 × HNO_3	Liu et al., (2019)
(2)	NO_2 + aerosol = 0.5 × HONO + 0.5 × HNO_3	Liu et al., (2019)
(3)	NO_2 + ground = HONO	Li et al., (2018), Liu et al., (2019)
(4)	NO_2 + ground + *hv* = HONO	Liu et al., (2019)

Table S2. Regional total emissions of gas and primary particulate matter in China in 2013 and 2021 and its decrease ratio from 2013 to 2021.

	SO_2	NO_x	NH_3	$PM_{2.5}$	VOCs
2013 (unit: kt)	22402	27753	11040	12536	25330
2021 (unit: kt)	5640	15096	8847	6445	22398
(2013-2021)/2013	75%	46%	20%	49%	12%

Table S3. Statistics for the simulation of meteorological factors in January and July of 2013 and 2021.

Meteorological factors		OBS	SIM	Bias
T2 (℃)	January 2013	269.23	269.10	-0.76
	January 2021	270.56	269.97	-0.59
	July 2013	298.02	297.16	-0.86
	July 2021	298.55	297.65	-0.90
Q2 (g/kg)	January 2013	2.47	2.38	-0.09
	January 2021	2.54	2.46	-0.09
	July 2013	14.86	14.71	-0.15
	July 2021	16.30	15.58	-0.72
WS10 (m/s)	January 2013	2.38	3.31	0.94
	January 2021	2.68	3.68	1.00
	July 2013	2.62	3.62	1.00
	July 2021	2.69	3.51	0.82
WD10 (°)	January 2013	275.99	282.83	10.27
	January 2021	259.21	251.70	11.46
	July 2013	192.27	183.08	4.86
	July 2021	180.47	157.43	3.96

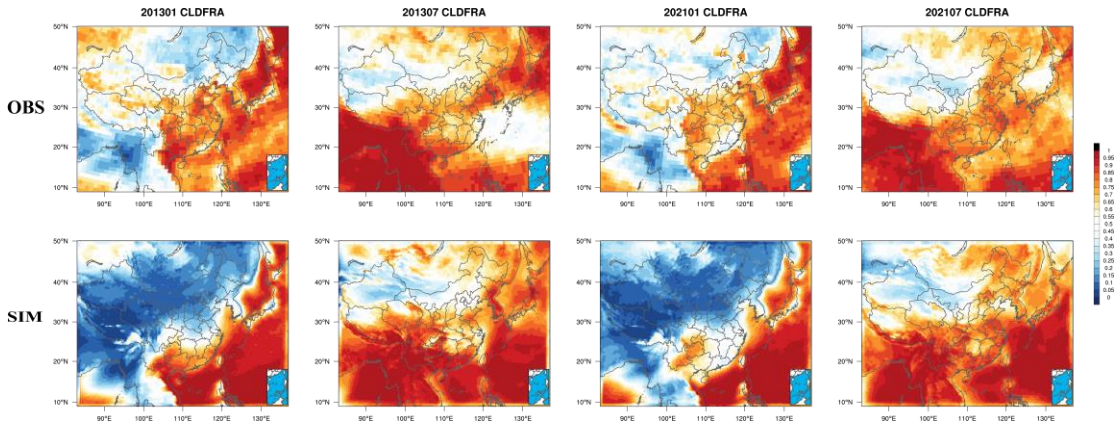

Fig. S1. Observation and simulation of cloud fraction in January and July of 2013 and 2021.

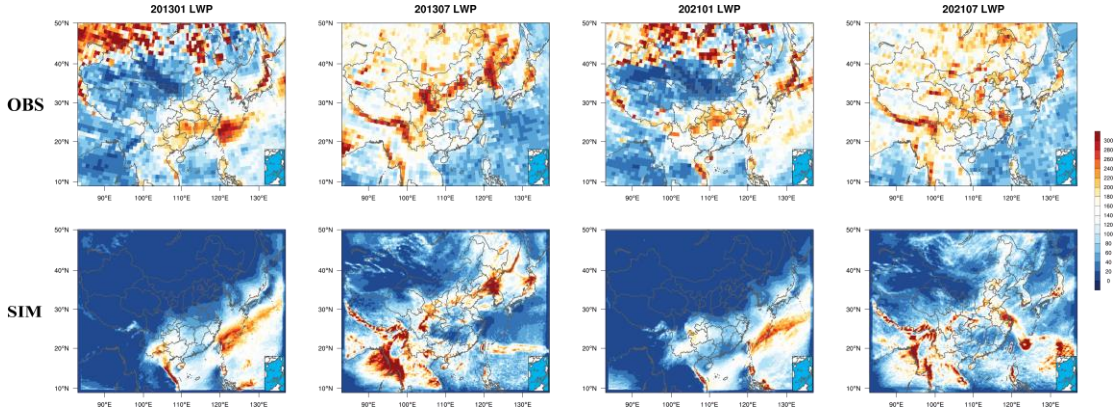

Fig. S2. Observation and simulation of liquid water path (unit: g m^{-2}) in January and July of 2013 and 2021.

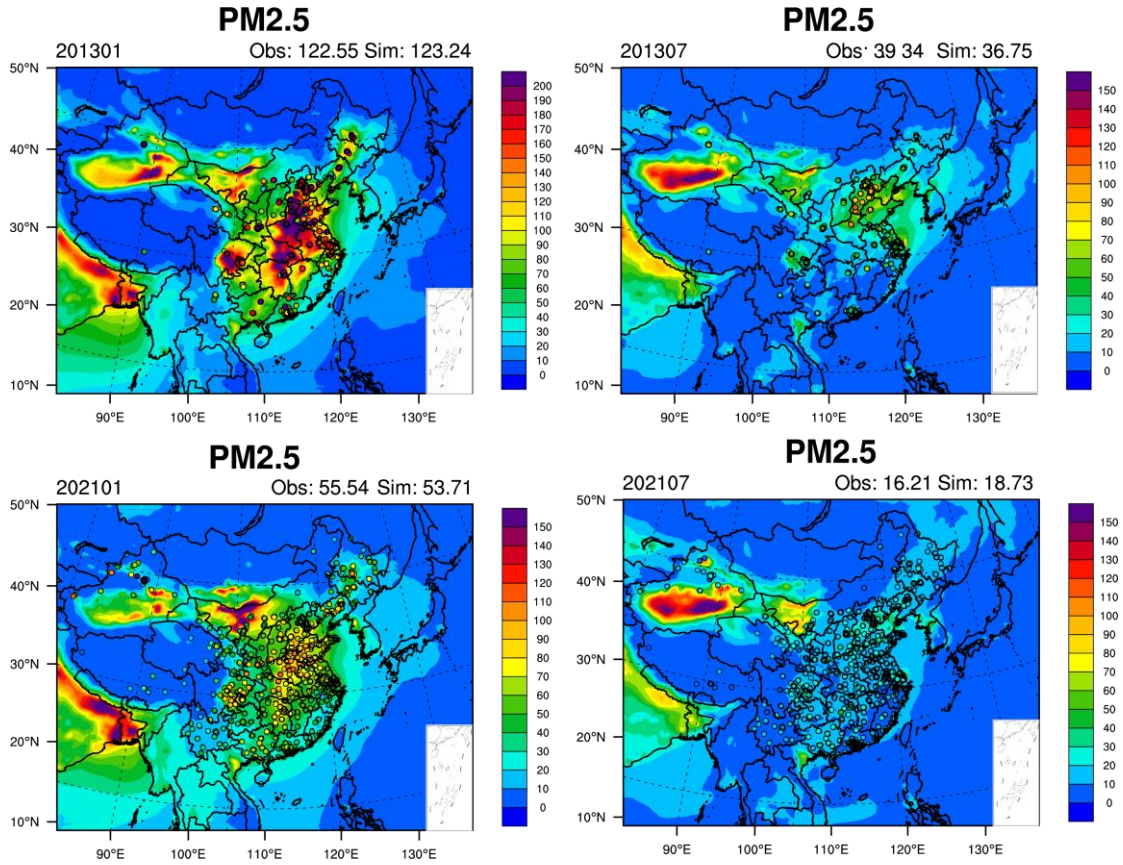

Fig. S3. Observation and simulation of surface $PM_{2.5}$ concentration (unit: $\mu g\ m^{-3}$) in January and July of 2013 and 2021.

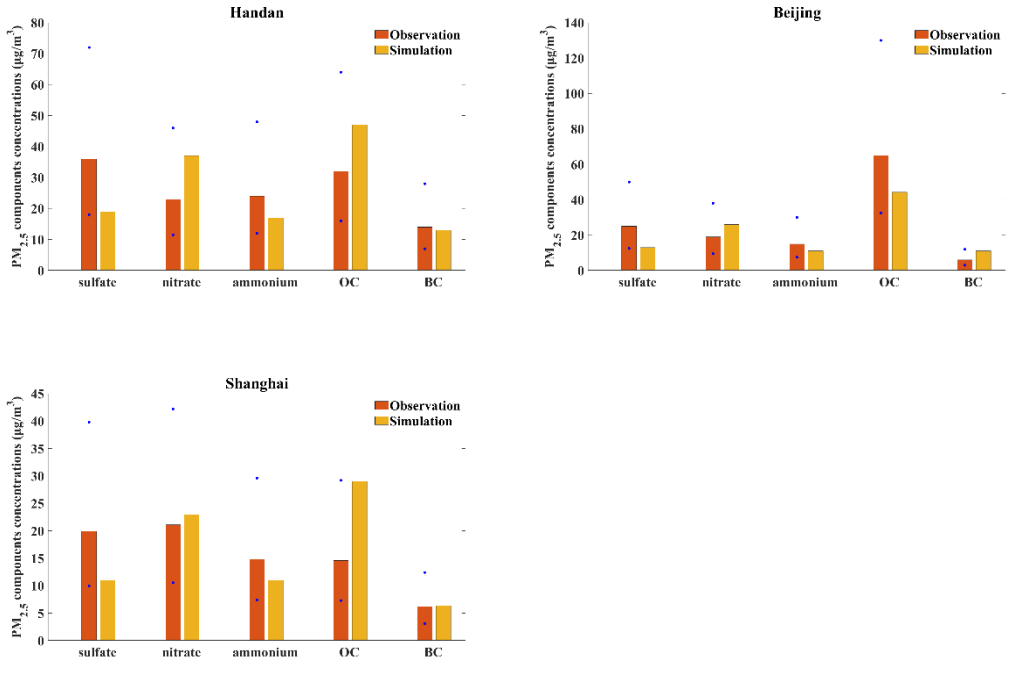

Fig. S4. Comparisons between $PM_{2.5}$ component observations and simulations in Handan, Beijing and Shanghai in January 2013. The blue points represent double or half of the $PM_{2.5}$ component observations. OC and BC represent organic aerosol and black carbon.

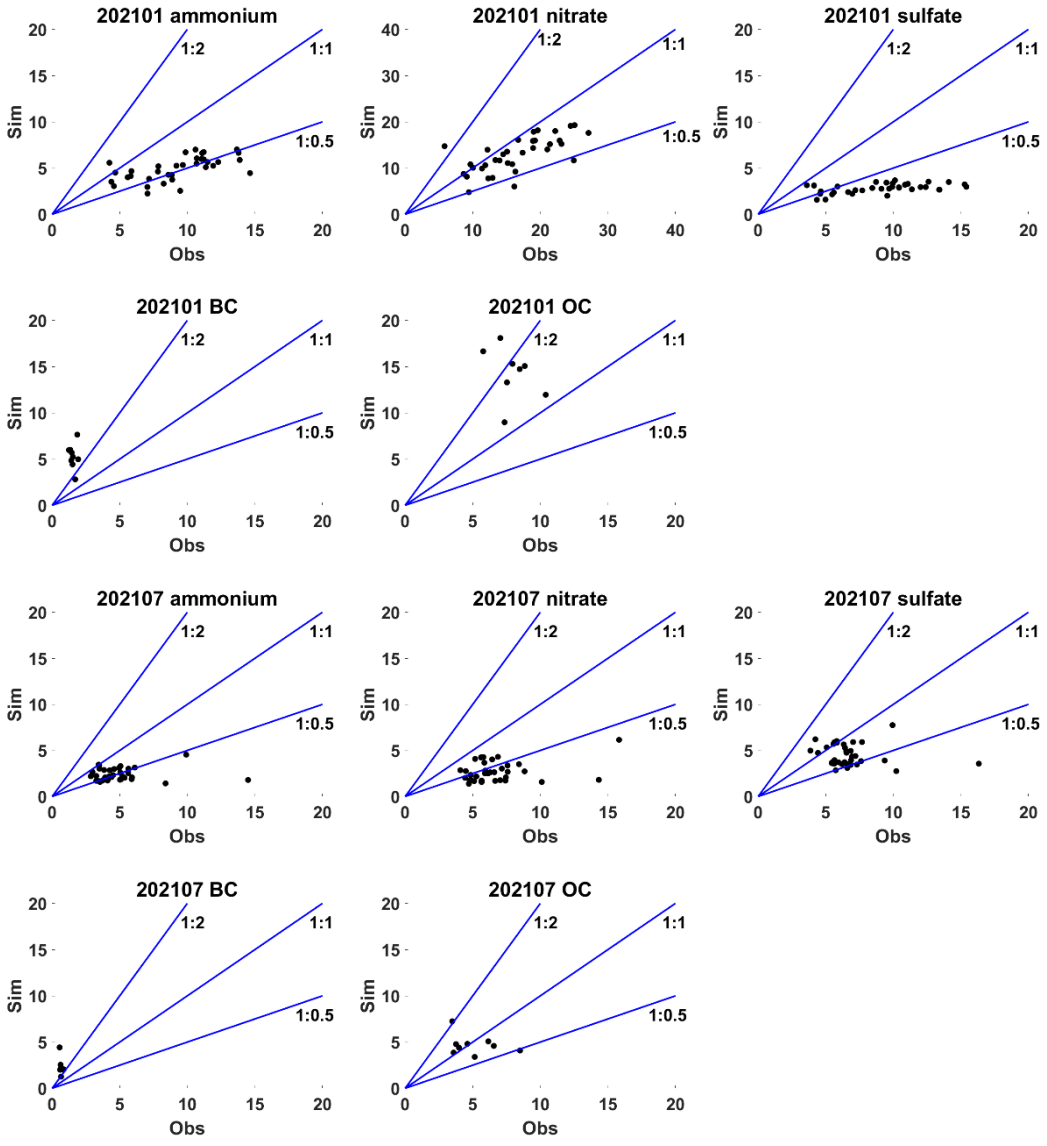

Fig. S5. The ratios of simulation to observation of ammonium, nitrate, sulfate, BC and OC (unit: $\mu g\ m^{-3}$) in January and July 2021.

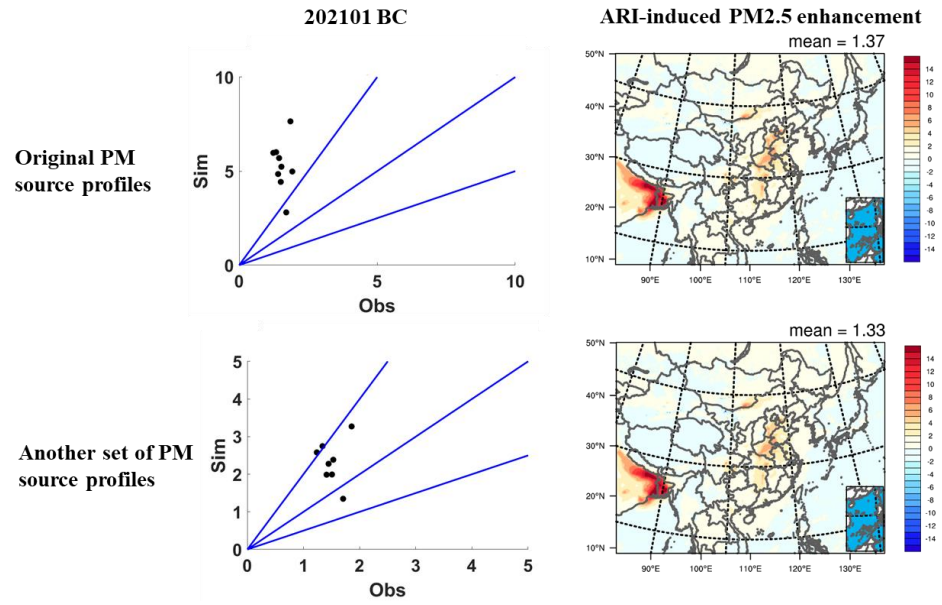

Fig. S6. The ratios of simulation to observation of BC and ARI-induced $PM_{2.5}$ enhancement (unit: μg m^{-3}) obtained from original PM source profiles and another set of PM source profiles in January 2021.

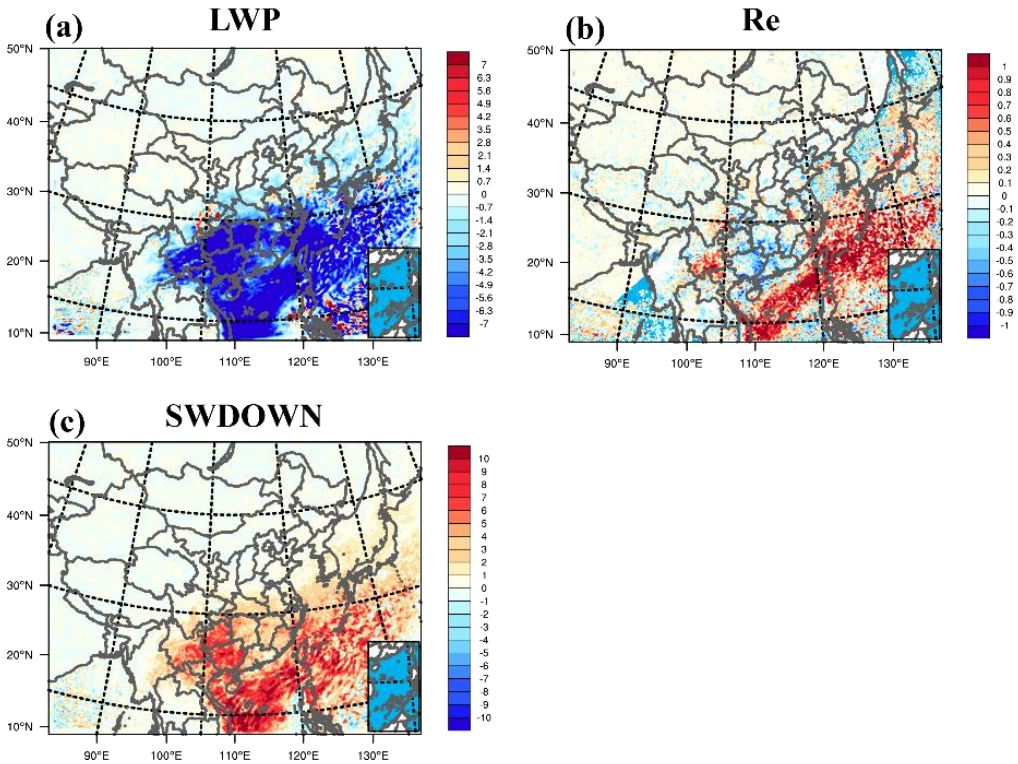

Fig. S7. Change in aerosol-induced liquid water path (LWP) (unit: g m^{-2}),

Re (unit: μm) and ACI-induced downward shortwave radiation at the surface (SWDOWN) reduction (unit: W m^{-2}) in January owing to the emission reduction from 2013 to 2021.

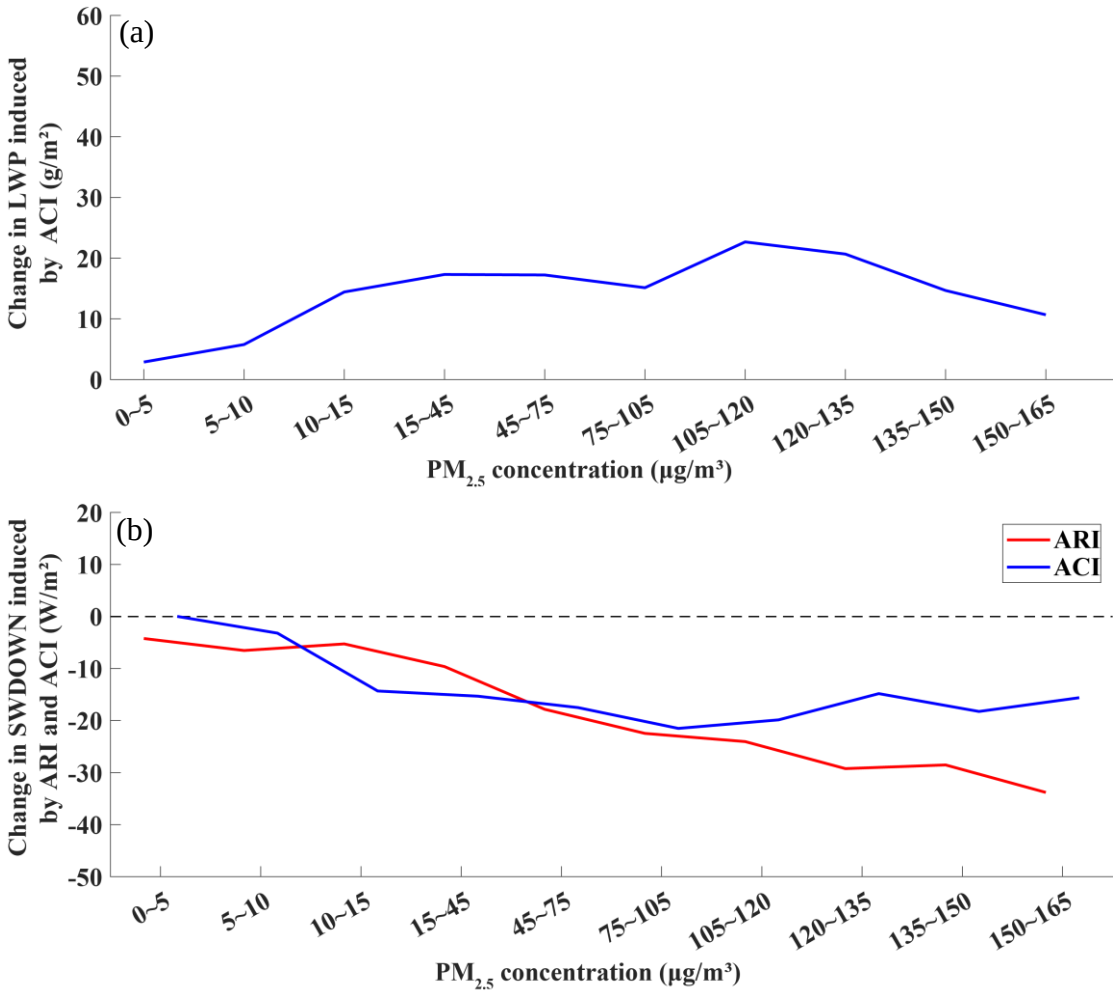

Fig. S8. Change in LWP induced by ACI and SWDOWN induced by ARI and ACI at different $PM_{2.5}$ levels.

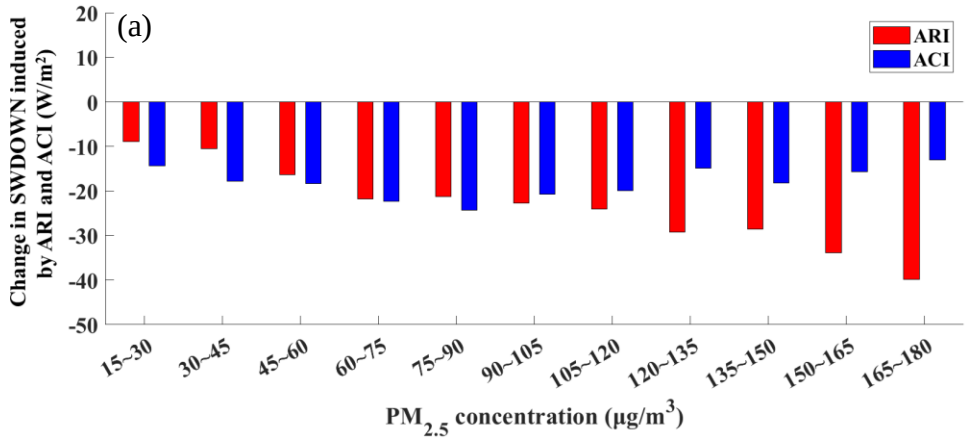
(a)
ARI
ACI
Change in SWDOWN induced by ARI and ACI (W/m²)
20
10
0
-10
-20
-30
-40
-50
15~30
30~45
45~60
60~75
75~90
90~105
105~120
120~135
135~150
150~165
165~180
PM2.5 concentration (μg/m3)

96

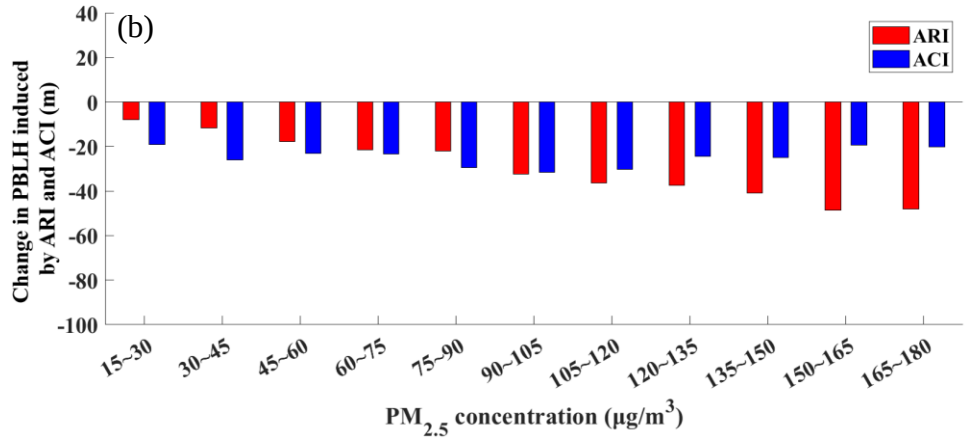
(b)
ARI
ACI
Change in PBLH induced by ARI and ACI (m)
40
20
0
-20
-40
-60
-80
-100
15~30
30~45
45~60
60~75
75~90
90~105
105~120
120~135
135~150
150~165
165~180
PM2.5 concentration (μg/m3)

97

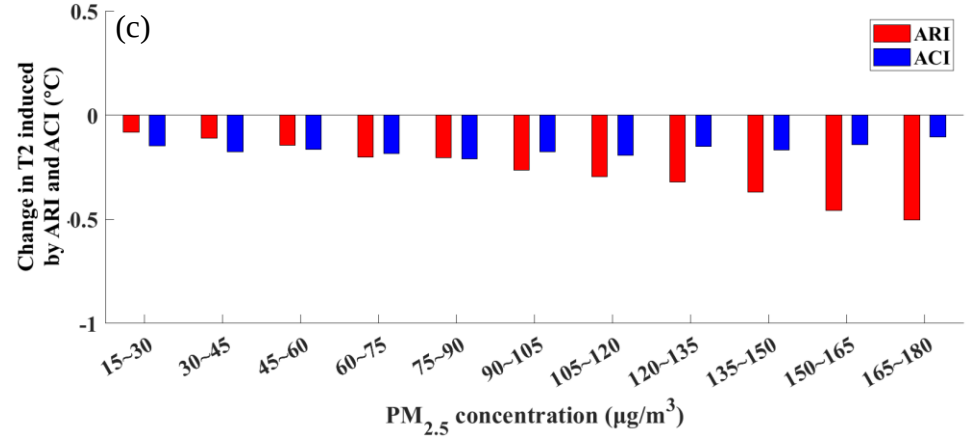
(c)
ARI
ACI
Change in T2 induced by ARI and ACI (°C)
0.5
0
-0.5
-1
15~30
30~45
45~60
60~75
75~90
90~105
105~120
120~135
135~150
150~165
165~180
PM2.5 concentration (μg/m3)

98

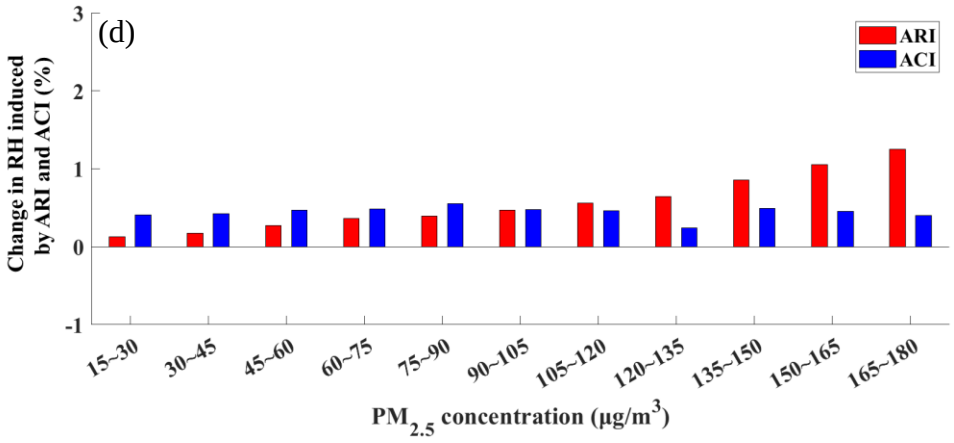

Fig. S9. Change in (a) SWDOWN, (b) planetary boundary layer height (PBLH), (c) air temperature at 2 m (T2), and (d) relative humidity (RH) induced by ARI and ACI at different ambient $PM_{2.5}$ levels. These data are from the simulations for January and July in the experiments of 21M13E and 21M21E.

References

Li, D. D., Xue, L. K., Wen, L., Wang, X. F., Chen, T. S., Mellouki, A., Chen, J. M., and Wang, W. X.: Characteristics and sources of nitrous acid in an urban atmosphere of northern China: Results from 1-yr continuous observations, Atmos Environ, 182, 296-306, 10.1016/j.atmosenv.2018.03.033, 2018.

Liu, Y. H., Lu, K. D., Li, X., Dong, H. B., Tan, Z. F., Wang, H. C., Zou, Q., Wu, Y. S., Zeng, L. M., Hu, M., Min, K. E., Kecorius, S., Wiedensohler, A., and Zhang, Y. H.: A Comprehensive Model Test of the HONO Sources Constrained to Field Measurements at Rural

North China Plain, Environ Sci Technol, 53, 3517-3525, 10.1021/acs.est.8b06367, 2019.

Wang, L. W., Wen, L., Xu, C. H., Chen, J. M., Wang, X. F., Yang, L. X., Wang, W. X., Yang, X., Sui, X., Yao, L., and Zhang, Q. Z.: HONO and its potential source particulate nitrite at an urban site in North China during the cold season, Sci Total Environ, 538, 93-101, 10.1016/j.scitotenv.2015.08.032, 2015.

Xue, C. Y., Zhang, C. L., Ye, C., Liu, P. F., Catoire, V., Krysztofiak, G., Chen, H., Ren, Y. G., Zhao, X. X., Wang, J. H., Zhang, F., Zhang, C. X., Zhang, J. W., An, J. L., Wang, T., Chen, J. M., Kleffmann, J., Mellouki, A., and Mu, Y. J.: HONO Budget and Its Role in Nitrate Formation in the Rural North China Plain, Environ Sci Technol, 54, 11048-11057, 10.1021/acs.est.0c01832, 2020.

Zhang, S. P., Sarwar, G., Xing, J., Chu, B. W., Xue, C. Y., Sarav, A., Ding, D. A., Zheng, H. T., Mu, Y. J., Duan, F. K., Ma, T., and He, H.: Improving the representation of HONO chemistry in CMAQ and examining its impact on haze over China, Atmos Chem Phys, 21, 15809-15826, 10.5194/acp-21-15809-2021, 2021.